Supplemental Materials and Methods

EMS mutagenesis

3-day old virgin males bearing a *ppk-CD4-tdTomato* insertion on chromosome 3 were starved for 6 hours and fed 0.025M EMS in 1% sucrose for 18 hours and used to generate a collection of balanced 3rd chromosome EMS-induced mutations that were subsequently analyzed for effects on dendrite growth using confocal microscopy.

Fly Stocks

The following alleles were used in this study (source in parenthesis; BL, Bloomington Stock Center): w^{118}, $path^{dg50}$ (this study), $path^{KG06640}$ (BL14607) $dTor^{\Delta P}$ (BL7014), sm^{YC0023} (BL50862), $CG5174^{CA07176}$ (BL50819), $G\alpha o^{CA06658}$ (Flytrap), $Ago1^{CA06914}$ (BL50805), $Imp^{ZCL0310}$ (Flytrap), $CG12163^{CC00625}$ (BL51538), Cam^{P00695} (BL50843), $\beta tub56^{DYC0063}$ (BL50867), $Tsp42Ed^{YC0084}$ (BL50869), $nrv2^{ZCL1649}$ (BL6828), $trol^{ZCL1973}$ (Flytrap), *ppk-CD4-tdGFP* (BL35845), *ss-myrGFP* (this study), *Df(3L)BSC773* (BL27345), *UAS-Path-A-GFP* (this study), *UAS-Path-C-GFP* (this study), *UAS-PathΔN-GFP* (this study), *UAS-PathΔC-GFP* (this study), *UAS-Rluc-Fluc* bicistronic reporter (this study), *UAS-rac* (BL6293), *UAS-PI3K92E* (BL8294), *UAS-Raf* (Peter Soba), *UAS-cut* (Yuh Nung Jan), *UAS-Tor(DN)* (BL7013), *UAS-Tor* (BL7012), *UAS-Rheb* (BL9688), *UAS-raptor* (53726), *UAS-Akt* (BL8191), *UAS-Akt-myr* (BL50758), *UAS-S6K* (BL6910), *UAS-S6K(CA)* (BL6912), *UAS-S6K(DN)* (BL6911), *UAS-RagA(DN)* (Thomas Neufeld), *UAS-eIF4e* (BL8710), *UAS-pum(RNAi)*, *UAS-RpL22(RNAi)*, *UAS-LAMP1-GFP* (BL42714), *UAS-Rab-7-YFP* (BL23641), *UAS-Rab11-GFP* (BL8506), *UAS-spin-RFP* (BL42716), *UAS-Rab4-RFP* (BL8505), *UAS-mCD8-GFP* (BL5137), *UAS-mitoGFP* (BL8442), *Actin-Gal4* (BL4414), *98b-Gal4* (this study), *ppk-Gal4* (Yuh Nung Jan), *221-*

Gal4 (Yuh Nung Jan), *109(2)80-Gal4* (BL8769), *HS-Gal4* (BL2077), *MHC-Gal4* (BL55132), *GMR23D11-Gal4* (BL45127), *elav-gal4* (BL458), *Frt40A* (BL1816, BL5192), *Frt2A* (BL1997, BL5190), *tub-Gal80* (BL5190, BL5192).

Immunohistochemistry

Larval fillets were dissected/processed as described (Grueber et al. 2002) with the exception of tissue for anti-Path staining, which was fixed in 10% TCA for 15 minutes, washed 5x in PBS-Triton-X100 (0.3%) and then processes as other tissue. Samples were stained with the following antibodies: HRP conjugated with Cy2 or Cy3 (1:200; Jackson ImmunoResearch), mCD8 (1:100; Life Technologies), anti-Path (1:500), anti-RpL22 (1:100; Kearse et al. 2011), anti-eIF4E (1:1500; Lachance et al. 2002), DAPI (50ng/mL; Life Technologies) and secondary antibodies from Jackson ImmunoResearch (1:250).

Microarray analysis

Microarrays were performed using previously described procedures (Jiang et al. 2014; Parrish et al. 2014) with minor modifications. For class IV da neurons, body wall filets of 3rd instar larvae were dissocated to single cell suspensions in PBS containing 1 mg/ml collagenase for 20 minutes at 37°C with automated mixing at 1000 rpm (Eppendorf Thermomixer). Samples were additionally triturated 10x through a P1000 pipette tip every 5 minutes during the incubation. Neurons were isolated by flow cytometry into 300 µl PBS using a FACSAria, and immediately re-sorted into 100 µl RNAqueous Micro Lysis buffer (Life Technologies). Samples were flick-mixed and immediately frozen on dry ice. RNA was isolated using the RNAqueous Micro kit as per the manufacturer's protocol, and RNA was amplified using two rounds of linear amplification using the Aminoallyl MessageAmp II kit (Life Technologies). Dye-coupled aRNA was fragmented

and hybridized to custom-designed 8x60k gene expression microarrays as per the manufacturer recommendations (Agilent Technologies). The microarrays used in these study were ported to the 8x60k platform and include all previous described probes (Parrish et al. 2014), with additional probes extending coverage to newly annotated genes, additional isoforms, and more non-coding RNAs. Details of the platform are available in the NCBI Gene Expression Omnibus under Accession number GPL19582, and all microarray data are publicly available under Accession number GSE64477. Microarrays were scanned on an Agilent scanner at 3 μm resolution as a 20-bit image, and probe intensities were extract using Agilent Feature Extraction. Raw Cy3 intensities were extracted and quantile normalized using limma (Smith 2005). Differentially expressed genes were identified using Significance Analysis for Microarrays (Tusher et al. 2001). Pairwise comparisons were performed with a false discovery rate of 1% and 2-fold change threshold. Hierarchical clustering and heatmap visualization were performed as previously described (Kim et al. 2012). For DAVID analysis, a Benjamini-corrected p value of 0.05 was considered significant. Intersectional analysis was performed using in-house Perl scripts to identify genes commonly increased or decreased in abundance in *path* mutants, relative to wild type, in C4da neurons and body walls.

Accessions

All microarray data is available in the NCBI Gene Expression Omnibus under accession number GSE64477.

References

Grueber WB, Jan LY, Jan YN. 2002. Tiling of the Drosophila epidermis by multidendritic sensory neurons. *Dev Camb Engl* **129**: 2867–2878.

Jiang N, Soba P, Parker E, Kim CC, Parrish JZ. 2014. The microRNA bantam regulates a developmental transition in epithelial cells that restricts sensory dendrite growth. *Dev Camb Engl* **141**: 2657–2668.

Kearse MG, Chen AS, Ware VC. 2011. Expression of ribosomal protein L22e family members in Drosophila melanogaster: rpL22-like is differentially expressed and alternatively spliced. *Nucleic Acids Res* **39**: 2701–2716.

Kim CC, Nelson CS, Wilson EB, Hou B, DeFranco AL, DeRisi JL. 2012. Splenic red pulp macrophages produce type I interferons as early sentinels of malaria infection but are dispensable for control. *PloS One* **7**: e48126.

Lachance PED, Miron M, Raught B, Sonenberg N, Lasko P. 2002. Phosphorylation of eukaryotic translation initiation factor 4E is critical for growth. *Mol Cell Biol* **22**: 1656–1663.

Parrish JZ, Kim CC, Tang L, Bergquist S, Wang T, Derisi JL, Jan LY, Jan YN, Davis GW. 2014. Krüppel mediates the selective rebalancing of ion channel expression. *Neuron* **82**: 537–544.

Smith GK. 2005. Limma: linear models for microarray data. In *Bioinformatics and Computational Biology Solutions Using R and Bioconductor* (eds. R. Gentleman, V. Carey, S. Dudoit, R. Irizarry, and W. Huber), pp. 397–420, Springer, New York.

Tusher VG, Tibshirani R, Chu G. 2001. Significance analysis of microarrays applied to the ionizing radiation response. *Proc Natl Acad Sci U S A* **98**: 5116–5121.

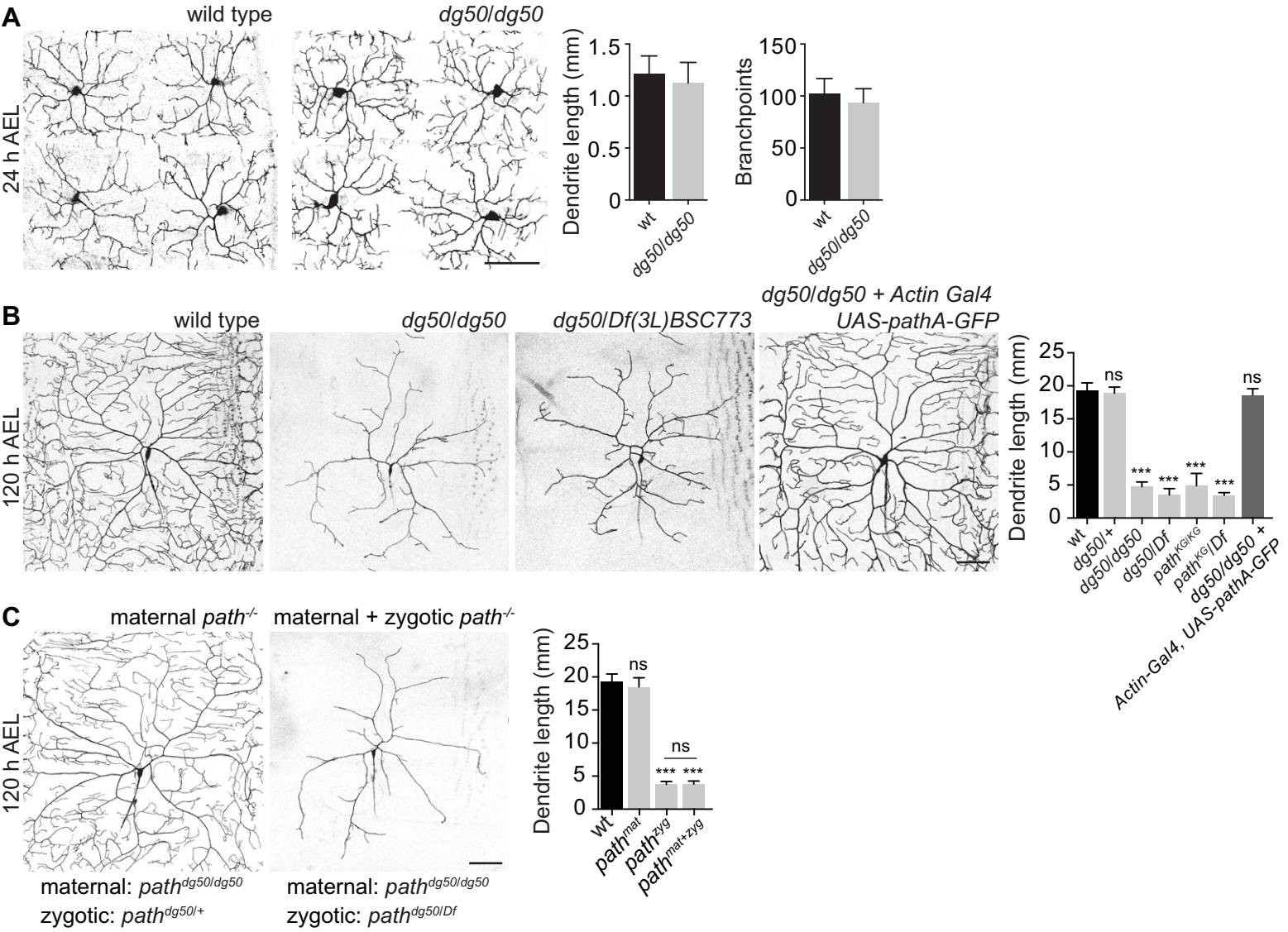

Figure S1. Supplement to Figure 1. (A) Early dendrite growth proceeds normally in dg50 mutants. Representative images of C4da neurons (*ppk-CD4-tdTomato*) in wt control and *dg50* mutants at 24 h AEL are shown. Quantification of dendrite length and branching is shown at right (n=8 neurons, each genotype). (B) *dg50* is a loss-of-function allele of *path*. Representative images of C4da neurons and quantification of dendrite length (mean and standard deviation) are shown for the indicated genotypes at 120 h AEL (n=8 neurons, each genotype). (C) Maternal *path* does not influence larval dendrite growth. Images of C4da neurons in larvae derived from $path^{dg50}$ germline clones are shown. In larvae with zygotic *path* function (left), no dendrite growth defects are apparent, whereas larvae lacking maternal and zygotic *path* (center) are indistinguishable from zygotic *path* mutants alone. Mean total dendrite length is shown for the indicated geneotypes. Error bars represent standard deviation. *n* = 8 neurons for each. ***P<0.001; ns, not significant relative to wt controls; one-way ANOVA with a post-hoc Dunnett's test. Scale bars, 50μm.

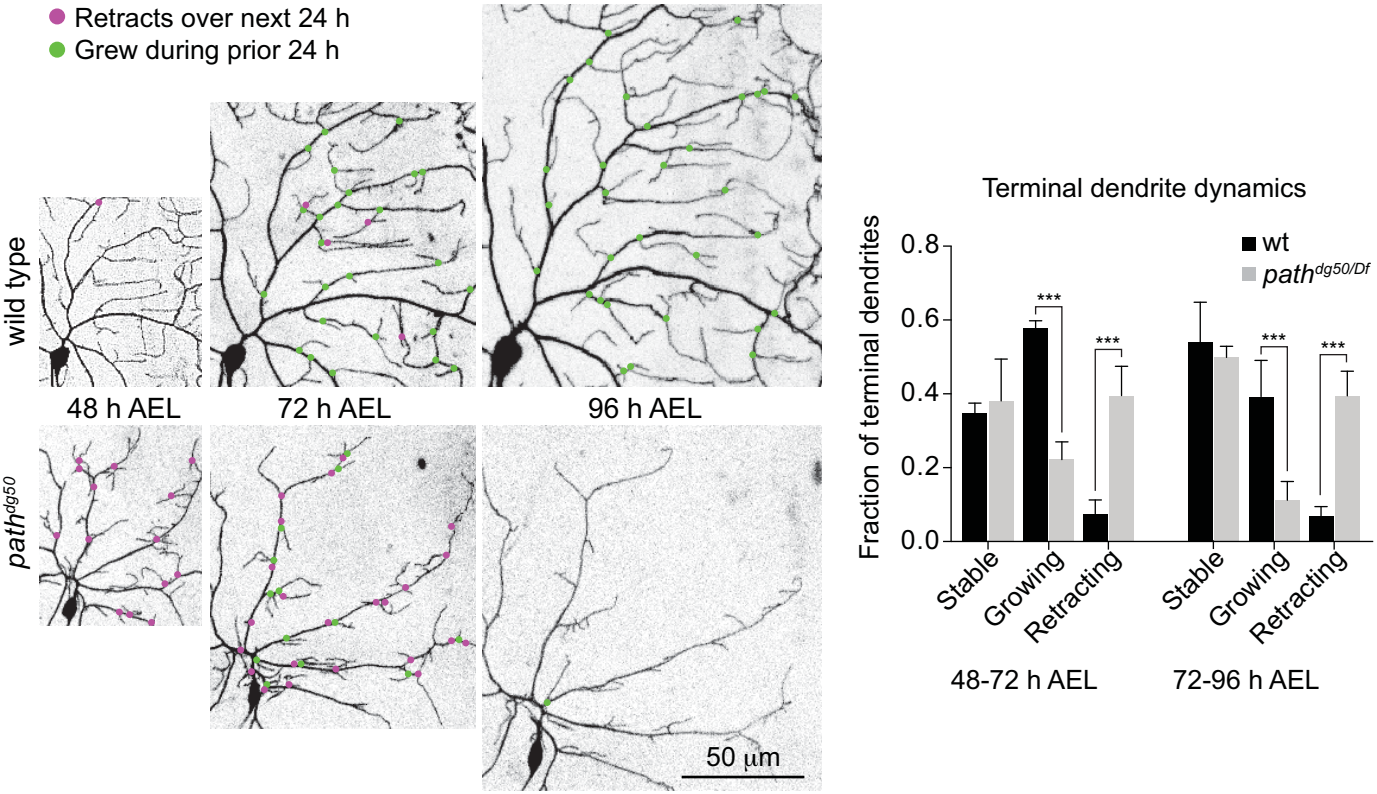

Figure S2. Supplement to Figure 1. Time-lapse analysis of dendrite branch dynamics in *path* mutants. C4da neurons (*ppk-CD4tdTomato*) from segment A3 were imaged at 48 h, 72 h, and 96 h AEL in wt control and *path*$^{dg50/Df}$ mutant larvae and terminal dendrite branch dynamics were monitored in the dorsal posterior quadrant of the arbor (corresponding to a 100x120 micron region of interest at 96 h AEL). To monitor dendrite dynamics, images of dendrite arbors from 2 time points (48-72 h and 72-96 h AEL) were overlayed, and terminal dendrites that exhibited changes in length >2µm were scored as dynamic terminals. Representative time-lapse series of wt and *path* mutant neurons are shown. Terminal branches that retract over the following 24 h period are marked at the base of the branch by a magenta circle and terminal dendrites that grew over the prior 24 h are marked by a green circle. 6 neurons each for wt and *path* mutants were imaged, and the proportion of stable, growing, and retractingterminal branches was calculated for each neuron. Mean values and standard deviation are shown. ***P<.001, one-way ANOVA with a post-hoc Tukey's test.

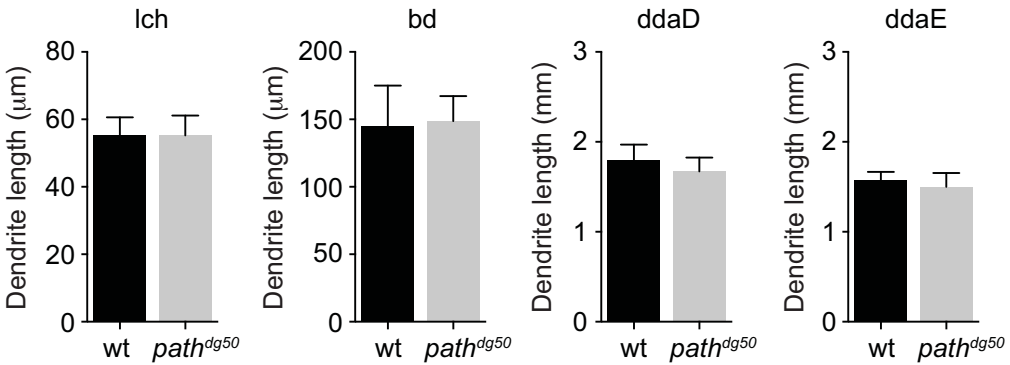

Figure S3. *path* is dispensable for dendrite growth in neurons with small dendrite arbors. Quantification of total dendrite length (mean and standard deviation) for lch, bd, ddaD, and ddaE MARCM clones is shown for the indicated genotypes. *n*>8 MARCM clones for each. Dendrite length not significantly differ between wt control and *path* mutant larvae for lch, bd, ddaD or ddaE neurons, unpaired t-test with Welch's correction.

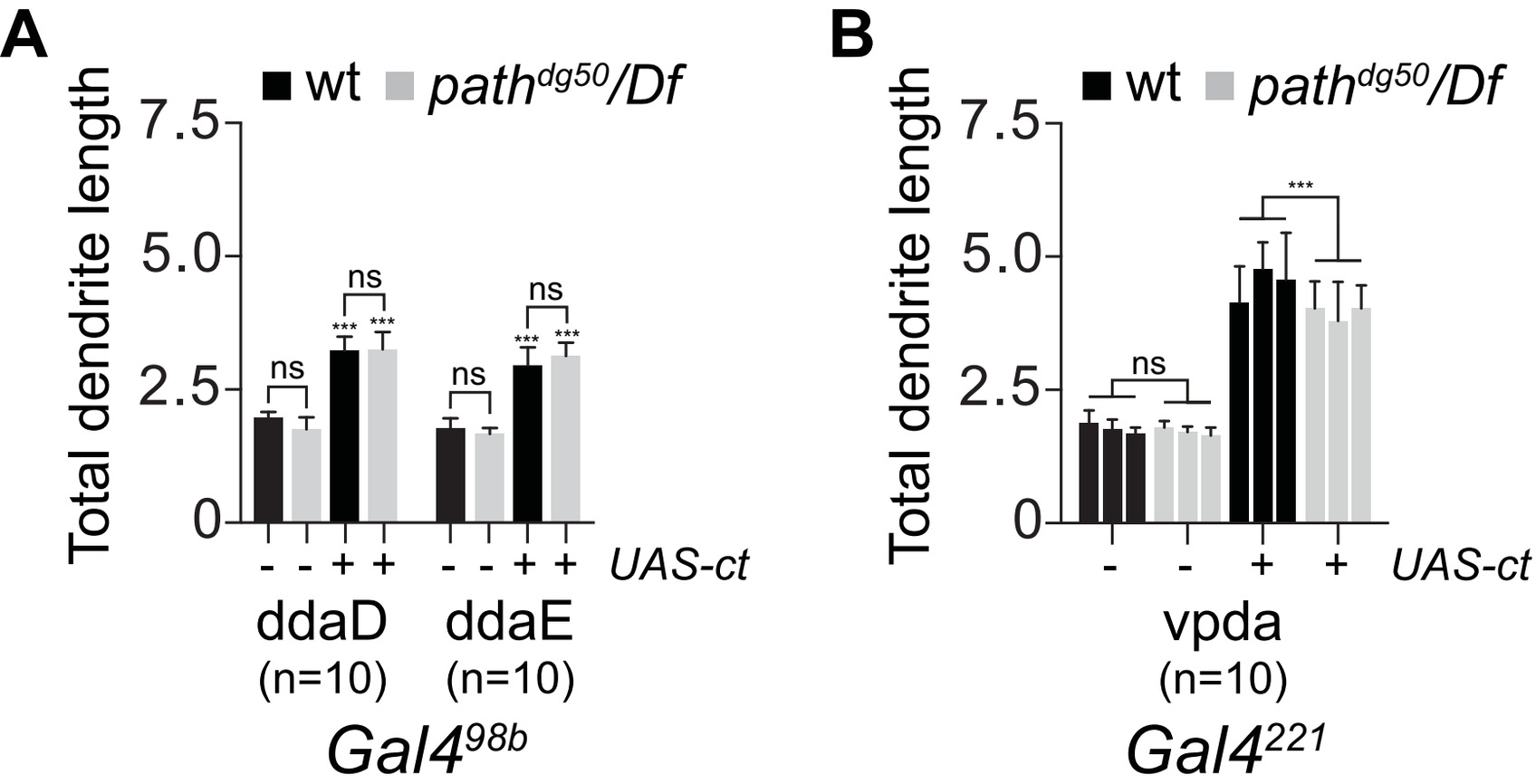

Figure S4. Supplement to Figure 2. Effects of *ct* overexpression on dendrite growth in class I neurons. (A) Total dendrite lenght for ddaD and ddaE in animals of the indicated genotype. (B) Total dendrite length for vpda in animals of the indicated genotype. Results from 3 independent experiments are shown (*n* = 10 neurons each bar). Bars represent mean values and error bars represent standard deviation. ****P*<0.001; ns, not significant; one-way ANOVA with a post-hoc Dunnett's test.

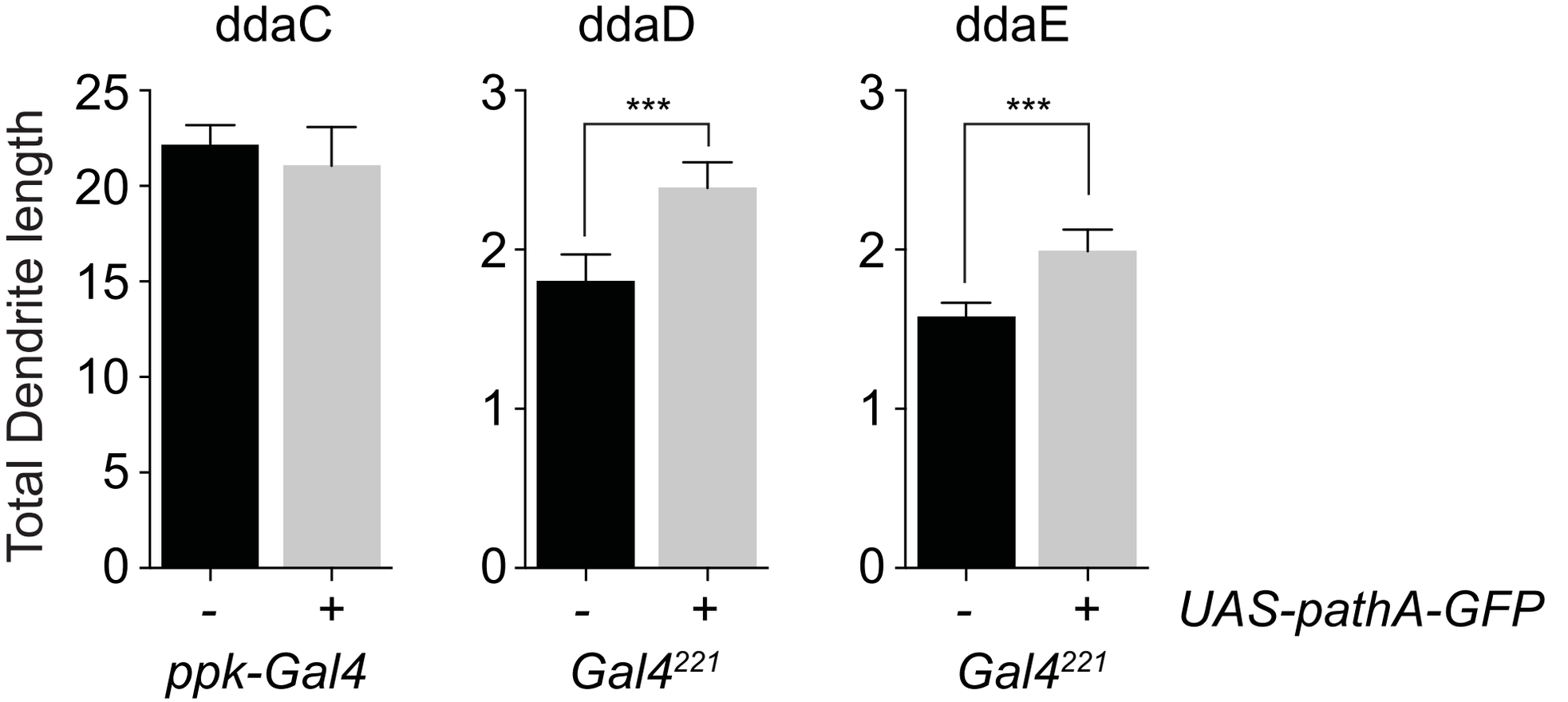

Figure S5. Overexpression of *path* can drive exuberant dendrite growth in neurons with small dendrite arbors. Quantification of total dendrite length for control (*Gal4/*+) or *path*-overexpressing (*Gal4/UAS-pathA-GFP*) C4da neurons (ddaC) and C1da neurons (ddaD and ddaE). Mean and standard deviation of measurments from *n*>8 cells are shown for each genotype. ****P*<.001, unpaired t-test with Welch's correction.

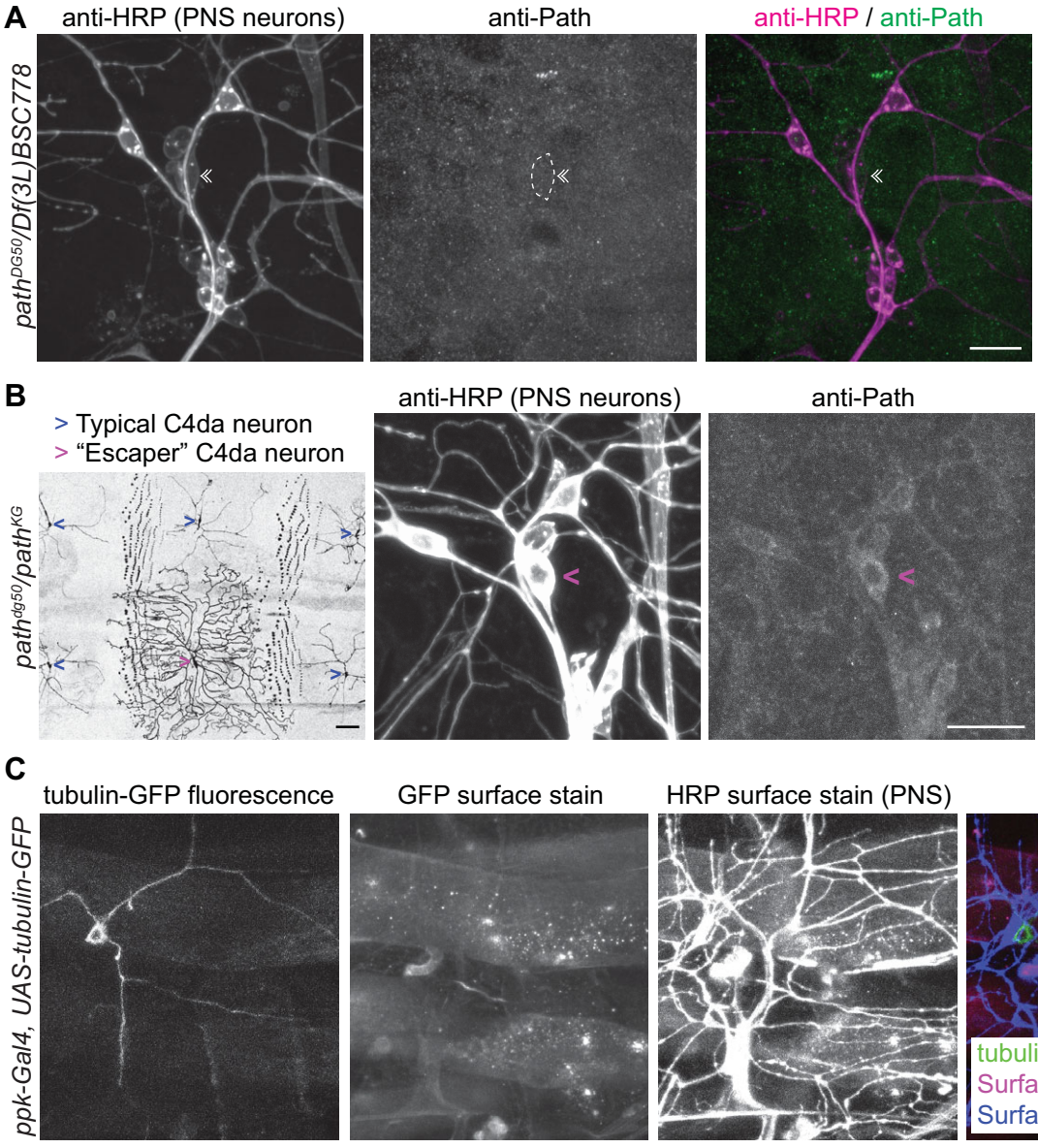

Figure S6. Supplement to Figure 4. (A) Specificity of anti-Path antibody. (B) Low levels of Path support dendrite growth. (B) An example of a rare "escaper" neuron in a *path* mutant larva (marked by the magenta carat) surrounded by neurons exhibiting the stereotypical *path* mutant growth defect (blue carats). Approximately 0.5% of C4da neurons exhibit normal growth in path mutant larvae, and these "escaper" neurons exhibit significant perdurance of Path protein. Anti-Path immunostaining of one such "escaper" neuron is shown, and levels (arbitrary units, AU) of Path immunoreactivity are shown for an escaper neuron and a typical *path* mutant neuron from adjacent segments in 10 different animals. Neurons from the same animal are connected by a line. (C) Control for surface staining. Total GFP fluorescence (after formaldehyde fixation), GFP surface stain (staining in non-permeabilizing conditions), and HRP surface staining (as a positive control) are shown for a C4da neuron expressing α-tubulin-GFP, which should not be surface exposed. Scale bars, 50 μm.

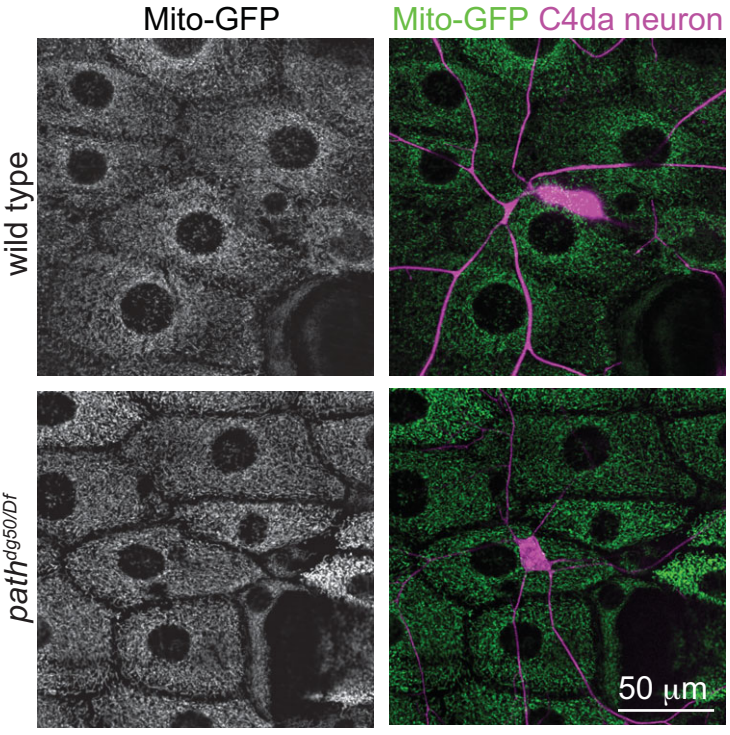

Figure S7. Supplement to Figure 6. Images of wild type or *path* mutant larvae expressing mitochondrial-targeted GFP in epithelial cells (*A58-Gal4, UAS-mitoGFP*) and Tomato in C4da neurons (*ppk-CD4tdTomato*). Whereas *path* mutant C4da neurons exhibit striking alterations in mitochondrial morphology (Fig. 6), wild type and *path* mutant larvae exhibit comparable epithelial mitochondria morphology.

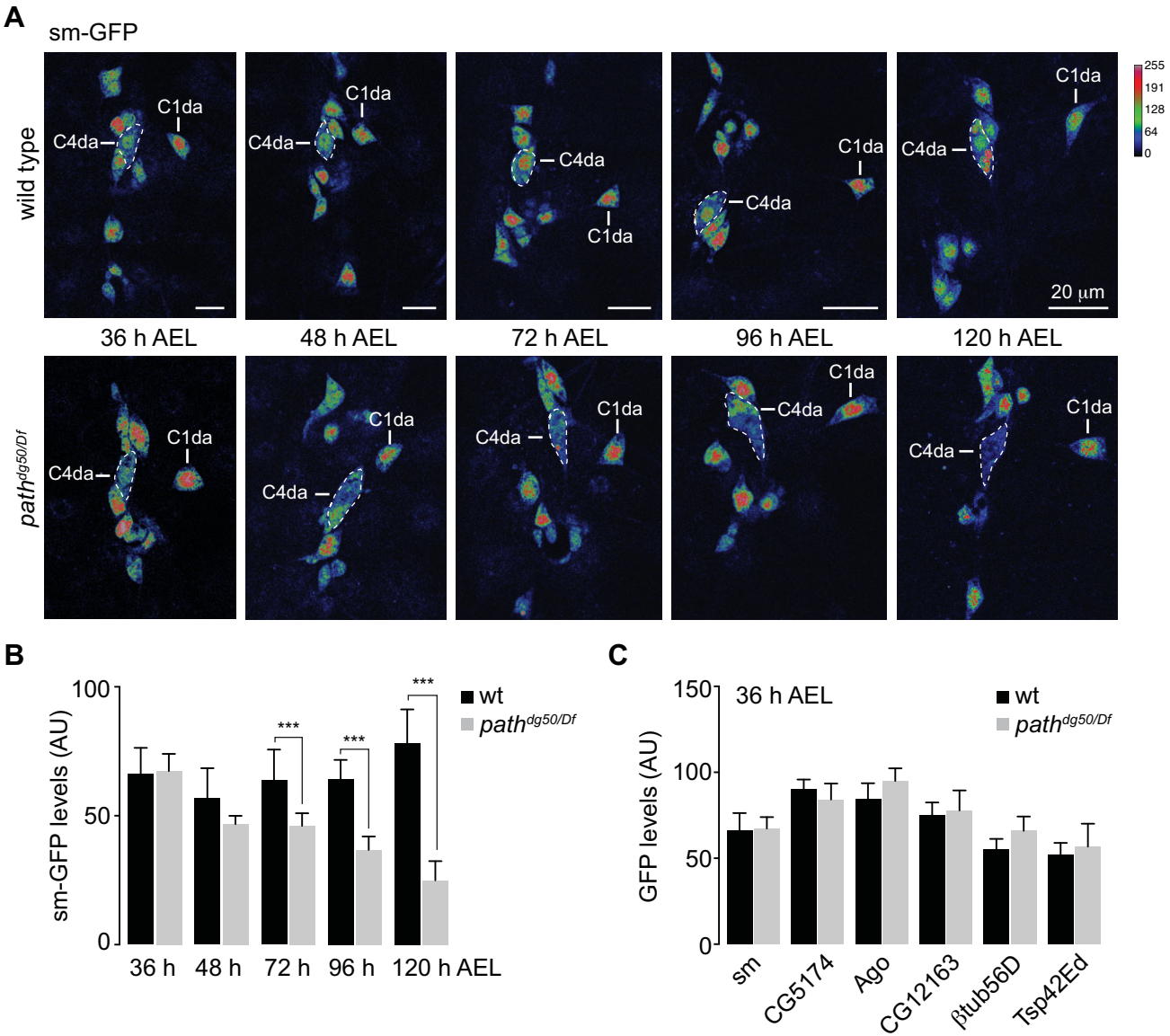

Figure S8. Supplement to Figure 6. (A) Time-course of sm-GFP expression in wild type control and *path* mutant larvae. C4da and C1da neurons are marked in each image and C4da neuron cell bodies are outlined with a white hatched line. All images were captured using live confocal microscopy and levels were assessed by measureing mean pixel intensity in cells of interest. Images are pseudocolored according to a lookup table (key, top right). (B) Plot depicting sm-GFP levels in C4da neurons over a developmental time-course in wt control and *path* mutant larvae. *n*>10 cells for each bar. ***P<.001 relative to time-matched wt control, one-way ANOVA with a post-hoc Tukey's test. (C) Plot depicting GFP levels for the indicated exon traps at 36 h AEL in wt control and *path* mutant larvae. *n*>10 cells for each bar. GFP levels for each of the exon traps did not significantly differ between wt control and *path* mutant larvae at 36 h AEL, unpaired t-test with Welch's correction.

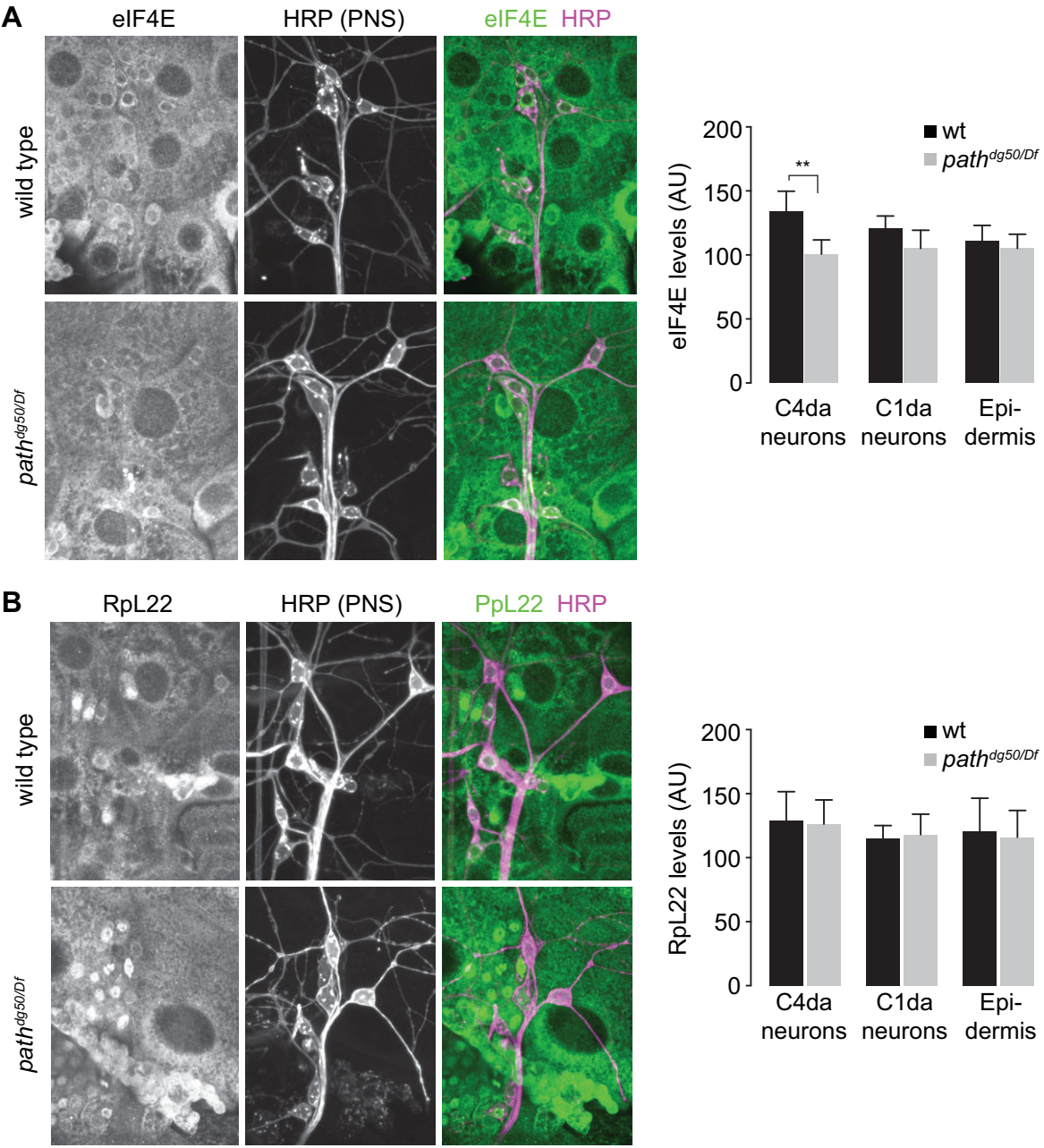

Figure S9. Supplement to Figure 7. (A) eIF4E and (B) Rpl22 levels in wild type control and *path*$^{dg50/Df}$ mutant larvae. Third instar larvae (96 h AEL) were stained with antibodies to eIF4E (A) or RpL22 (B) and HRP (to label PNS neurons). eIF4E (A) and Rpl22 (B) signal intensities were measured in 2D projections of confocal stacks. Control and *path* mutant fillets were processed identically (stained in the same tube, imaged using identical settings). Mean values and standard deviation for intensity measurements of 10 cells for each cell type/genotype combination shown. ***P<.001, one-way ANOVA with a post-hoc Tukey's test.

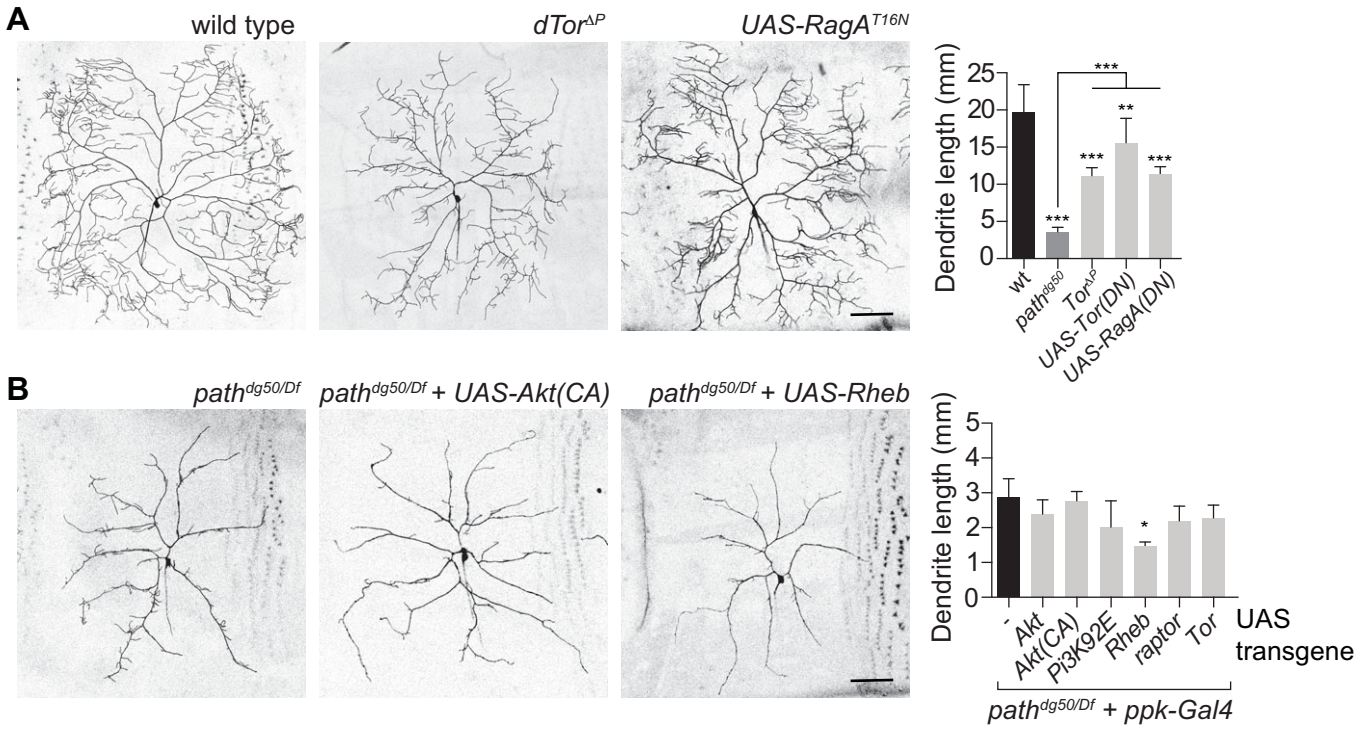

Figure S10. Supplement to Figure 7. Relationship between Path and TORC1 in dendrite growth. (A) Effect of TORC1 inactivation on C4da dendrite growth. Representative images of wild type control, *dTor* mutant, or RagA dominant-negative expressing C4da MARCM clones are shown. Quantification depicts mean total dendrite length for the indicated genotypes ($n > 6$ neurons for each). (B) Assaying rescue activity of TORC1 activation on C4da growth defects in *path* mutants. The indicated transgenes were expressed in C4da neurons of *path* mutants. Quantification depicts mean total dendrite length for the indicated genotypes ($n > 8$ neurons for each). *$P<0.05$; **$P<0.01$; ***$P<0.001$; ns, not significant; one-way ANOVA with a post-hoc Dunnett's test. Scale bars, 50μm.